Optimal tuning of the contour analysis method to recognize aircraft on remote sensing imagery

E N Dremov[1], S Yu Miroshnichenko[1] and V S Titov[1]

[1]South-West State University, 50 Let Oktyabrya street, 94, Kursk, Russia, 305040

e-mail: evgeni-dremov@yandex.ru, oldguy7@rambler.ru, titov-kstu@rambler.ru

Abstract. In this paper, we describe the experimental results of aircraft recognition on optical remote sensing imagery using the theory of contour analysis. We propose the a method to calculate optimal values of the contour's items quantity and the classification threshold through measuring within- and between-class distances for all possible training set instances combinations with followed by detection and minimization of the type I and II errors. We discuss the construction of contours' similarity measures combining the principles of finding the most appropriate reference instance and calculating the average value for the whole class. It is shown that the proposed parameters' tuning method and the similarity function make contour analysis capable to train on compact non-uniform datasets and to recognize aircraft on the noisy and less detailed images.

1. Introduction

The mathematical apparatus of contour analysis is an effective approach to solve the problem of objects recognition using their shapes as the distinctive features [1,2].

To reach affine transformation invariance researchers in the field of aircraft recognition use a combination of few features and methods such as contours, Zernike moments and wavelet coefficients in [3], Radon transform, PCA and kNN classification in [4], HOG, graph theory and an object reconstruction in [5].

In contrast, contour analysis uses the single similarity measure of two vector-contours, the module of the normalized dot product (NDP) that is invariant (insensitive) to transfer, rotation, and proportional scaling of the recognized object towards the reference one. The similar recognition methods produce a unique value per each classes pair [6-8] and require an additional clustering procedure to match an object to a certain class. In contrast, the NDP module provides a uniform similarity measure of two contours within the range [0..1] where 1 – denotes the identical instances. Moreover, the NDP itself is a complex-valued number describing contour's scale and rotation angle relatively the reference instance.

Despite the listed above advantages, the NDP has its own limitations, which include the need to select the values of the vector-contour's items quantity and the classification threshold used to decide whether the corresponding object belongs to a certain class.

The first limitation is a consequence of the fact that in order to calculate the NDP value, the compared contours should have the same items' quantity (however, the length of the vector-contours - the sum of its vectors lengths - does not have to be equal). The problem of optimal vector-contour's

items quantity selection is to find a balance between the lower values, smoothing together little-informative details and distinctive features of the recognized object, and higher values, providing more distinctive features but making the instances the single class more unlike [6].

The second limitation arises from the of the classification rule used to decide whether a given vector-contour belongs to one of the classes and consists in the need to select a threshold value corresponding to the minimal similarity value between the reference objects. This value for each class is determined by the differences between the instances in the training dataset.

Comparing to the state-of-the-art convolutional neural networks (CNN) [9, 10], requiring hundreds of images to train, contour analysis's based recognition methods are capable of dealing with compact and nonuniform datasets containing less than 10 instances per class. Moreover, CNNs require transfer learning techniques [11] to operate on images with spectral parameters different from the training ones (for example, created by the sensor of another type). To the contour analysis list of disadvantages, we should write a much shorter range of applications, as the recognition process is driven by the only feature – the object's shape, together with the strong addiction to the segmentation method's quality used to extract the object from an underlying surface [12-15].

This article considers the application of the mathematical apparatus of contour analysis to recognize the aircraft's class on remote sensing imagery. The shape of the aircraft on view from above is the primary distinctive feature determining its class. However, aircraft instances of the same class can have differences in shape due to the following reasons: the presence or absence of the external wing-mounted armament or equipment, the disassembly of aerodynamic surfaces (slats, flaps, rudders), engines and rotary blades, wings with variable geometry, folded wings for naval aircraft. Shape variations can also be caused by the segmentation algorithms that incorrectly react to the boundaries of its illuminated and shaded areas, as well as closely located airfield equipment.

The article has the following structure. Section 2 contains a formal statement of the recognition problem used to determine the list of optimized parameters. Section 3 is devoted to the description of the features of the training and test datasets: the first one serves as a data source to calculate optimal values of the parameters, the second one – to verify results. Section 4 shows the process and the results of the experiment to obtain the value of the classification threshold for each class in training dataset. Section 5 is devoted to the results of the experiment to determine the values of the vector-contour's items quantity required to calculate the NDP value for each class. Section 6 describes the selection of similarity value calculation criterion and the experimental results of the tuned contour analysis method. Section 7 contains a discussion and suggestions for future work.

2. Formalization of the recognition problem

We introduce the following notation:

$\mathbf{C} = \{C_i\}_1^{N_C}$ – is a set of aircraft classes, where C_i – is an aircraft class with index i, N_C – is the number of aircraft classes.

$\mathbf{\Gamma}_i = \left\{\Gamma_{ik}\right\}_{k=1}^{Ni}$ – is a set of reference vector-contours (hereinafter referred to as "references") of *i*-th class, *k* – is an reference instance index, N_i – is the number of instances in the *i*-th class, Γ_{ik} – instance contour of *i*-th aircraft class with index *k*.

Each instance described by a vector-contour Γ_{ik}, consisting of *l* complex-valued elements called elementary vectors $\gamma_{ik}(\cdot)$, designated as:

$$\Gamma_{ik} = (\gamma_{ik}(1), \gamma_{ik}(2), ..., \gamma_{ik}(l)).$$

The mathematical apparatus of contour analysis is applicable only to contours with the equal items quantity. In practice, images contain objects that have contours with an arbitrary number of elements. The process to transform the vector-contour to have strictly *l* elements is called "equalizing" [2]:

$$\Gamma_{ik} \xrightarrow{f_e} \Gamma_{ik}(l), \Gamma_{ik}(l) = \{\gamma_{ik}(n)\}_1^l. \quad (1)$$

The NDP $\eta(\cdot)$ is calculated by the formula:

$$\eta(\Gamma_{ik},\Gamma_{jm},l)=\frac{\left(\Gamma_{ik}(l),\Gamma_{jm}(l)\right)}{|\Gamma_{ik}(l)|\cdot|\Gamma_{jm}(l)|},\ \left(\Gamma_{ik}(l),\Gamma_{jm}(l)\right)=\sum_{n=1}^{l}(\gamma_{ik}(n),\gamma_{jm}(n)), \quad (2)$$

where $\Gamma_{ik}(l)$ and $\Gamma_{jm}(l)$ – are equalized vector-contours, $\left(\Gamma_{ik}(l),\Gamma_{jm}(l)\right)$ – is a vector-contours dot product, $|\Gamma_{ik}(l)|$ and $|\Gamma_{jm}(l)|$ - the norms (lengths) of the corresponding vector-contours.

The operations (2) and (3) with vector-contours are both performed on vectors of complex-valued numbers, which allows achieving the following features [1,3]:

1. The sum of the elementary vectors of a closed contour is zero.
2. Invariance to the transfer (Figure 1): the vector contour does not depend on the parallel transfer within the original image.
3. Invariance to the rotation (Figure 1): rotating an image by a certain angle is equivalent to rotating each elementary vector by multiplying it by a complex factor.
4. Invariance to scaling (Figure 1): changing the image size is equivalent to multiplying each elementary vector by the real scale factor.
5. Changing the starting point leads to a cyclic shift of the vector contour. The NDP is not invariant to the change of the initial point.

The later feature requires to transform the NDP to the cross-correlation function (CCF) of vector-contours, which in addition to the invariance properties of (2) is insensitive to the initial point's shift:

$$\tau(i,j,k,m,l)=\max_{s}\left|\frac{\left(\Gamma_{ik}(l),\Gamma_{jm}^{(s)}(l)\right)}{|\Gamma_{ik}(l)||\Gamma_{jm}(l)|}\right|, \quad (3)$$

where $s=0,...,l-1$ is a shift from to the initial point, $\Gamma_{jm}^{(s)}(l)$ – is a contour obtained from $\Gamma_{jm}(l)$ by the cycle shift of its elementary vectors to *s*-elements.

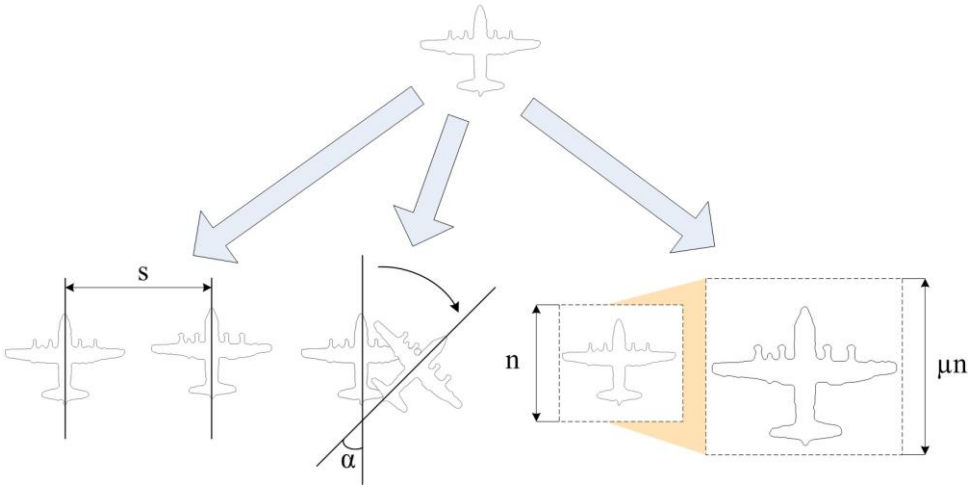

Figure 1. NDP invariance to the transfer, rotation, proportional scaling.

The classification rule to determine the affiliation of a certain contour Γ to C_i class is:

$$C(\Gamma)=\begin{cases}C_i: i=\arg\left[\max_i(f(\Gamma,\mathbf{\Gamma}_i)\geq T_i)\right],\\ \varnothing: \forall i\ \max_i f(\Gamma,\mathbf{\Gamma}_i)<T_i,\end{cases} \quad (4)$$

where T_i – is the classification threshold value for the aircraft of the *i*-th class, $f(\Gamma,\Gamma_i)\in[0,1]$ – is the function for calculation the similarity value of the given vector-contour Γ to the set $\mathbf{\Gamma}_i$ of reference objects.

The function for similarity value calculation can apply one of the two following criteria:

1. Maximum CCF for a vector-contour Γ and one of the reference instances Γ_{ik}:

$$f_1(\Gamma, \mathbf{\Gamma}_i) = \max_{k,s} \left| \frac{\left(\Gamma(l_i), \Gamma_{ik}^{(s)}(l_i)\right)}{|\Gamma(l_i)||\Gamma_{ik}(l_i)|} \right|, \quad (5)$$

where l_i - is the optimal value of the vector-contour's items quantity for *i*-th aircraft class.

2. The mean CCF value for a *i*-th whole class:

$$f_2(\Gamma, \mathbf{\Gamma}_i) = \frac{1}{N_i} \sum_{k=1}^{N_i} \max_{s} \left| \frac{\left(\Gamma(l_i), \Gamma_{ik}^{(s)}(l_i)\right)}{|\Gamma(l_i)||\Gamma_{ik}(l_i)|} \right|. \quad (6)$$

The aim of the article is to create a contour analysis tuning method by the solution of the following problems:

1. Determine the optimal values of the vector-contour's items' quantity $\mathbf{L} = \{l_i\}_{i=1}^{N_C}$ and the classification threshold $\mathbf{T} = \{T_i\}_{i=1}^{N_C}$ in terms of the minimum total number of I and II type errors.

2. Select a criterion to calculate the similarity value of the vector-contour to a set of reference instances $\mathbf{\Gamma}_i$.

3. Dataset details

The dataset we used within the experiment is divided into the training part, used to tune the recognition method's parameters and the test part for the verification.

The training dataset contains aerial images of optical range with a resolution of 0.15 m / pixel displaying the parking of decommissioned and reserved aircraft at the Davis-Monthan airfield [16]. The training dataset is compact and includes 430 images of the aircraft of eight classes: B-1, B-52, C-5, C-37, C-130, C-135, P-3, and S-3.

Figure 2 shows the examples of all 8 aircraft classes of the training dataset. Table 1 lists the characteristics of the classes and the instances' contours.

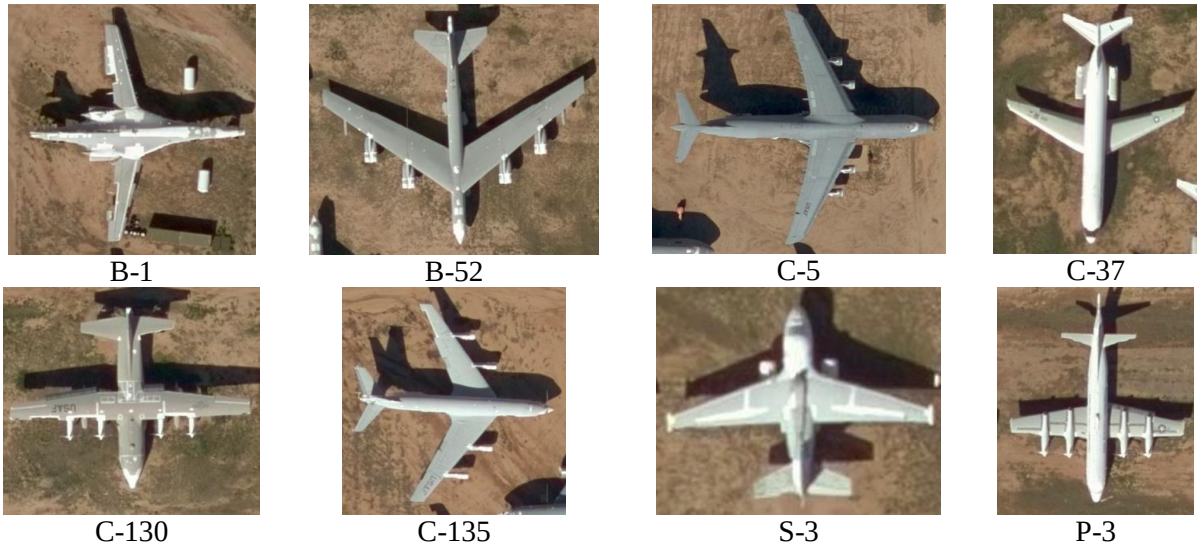

Figure 2. Image examples of aircraft in the training dataset.

The classes of the training dataset differ significantly from each other both in the number of instances and in the degree of within-class similarity of their contours. An example of a significant difference in the instances is shown in Figure 3 for B-1 class: the nose cone (Figure 3a), the engines (Figure 3b), the slats, flaps, landing shields, rudders, stabilizers (Figure 3c, d) were removed. The other classes (for instance, B-52) have minimal differences in instances.

The described differences in the training dataset require to calculate the optimal values of vector-contours' items quantity and the classification threshold individually for each class.

The test dataset is equivalent to the training one and contains 421 aerial images of three resolution levels: 0.15 (10 images), 0.3 (10 images) and 0.5 meters per pixel (402 images), shot in the Davis-

Monthan and a few operating airfields. Figure 4 shows the examples of the aircraft included in the test dataset (the details of the test dataset are given in Table 2).

Table 1. Characteristics of contours in the training dataset.

Aircraft class	B-1	B-52	C-5	C-37	C-130	C-135	P-3	S-3
Instances count	17	10	20	11	135	81	92	64
Mean items' quantity	1132	1945	2404	1227	1570	1420	1458	1132
Items' quantity histogram	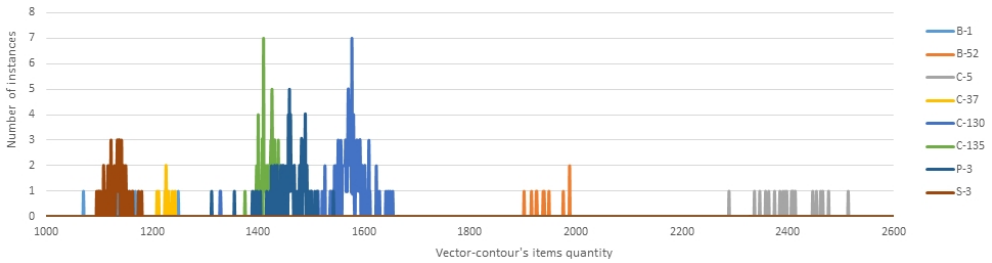							

a)  b)  c)  d) 

Figure 3. Instances of B-1 aircraft having various dismantled elements.

B-1 B-52 C-5 C-37

C-130 C-135 S-3 P-3

Figure 4. Images examples of the aircraft in the test dataset.

Test images of 0.3 and 0.5 meters per pixel (for instance, B-1 and C-130 on Figure 4) have significant visual differences from the training set in contrast and brightness as well as in lighting/shading scheme so the major remaining recognition feature is the shape. Test images of 0.15 meters per pixel were shot on the other season, have greater camera-to-surface angle, differences in color rendition and contain much more noise that seems to be caused by the lossy compression. All the described features of the test dataset strongly affect aircraft contours challenging the robustness of the proposed contour analysis's parameters tuning method.

Table 2. Characteristics of contours in the test dataset.

Aircraft class	B-1	B-52	C-5	C-37	C-130	C-135	P-3	S-3
Instances count	7	6	48	11	57	102	142	49
Mean items' quantity	1263	1884	2441	1177	1483	1315	1345	1084
Items' quantity histogram	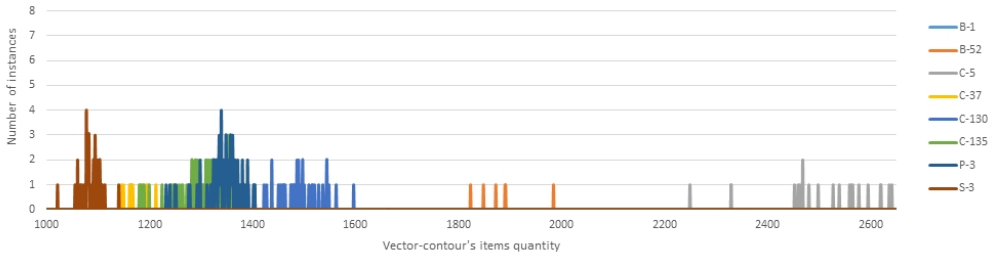							

4. Optimal classification thresholds calculation

To calculate the optimal classification thresholds $\mathbf{T}=\{T_i\}_{i=1}^{N_C}$, the measurements of within-class and between-class distances were made for all possible combinations of training dataset instances.

The measurement of the within-class distance is a calculation of the CCF (3) for a particular non-coincident pair of vector-contours of the same class. The measurement of a between-class distance is a calculation of CCF for a particular pair of vector-contours of different classes.

An error of a within-class distance measuring (type II error or a false negative measure) [17] is the value of within-class distance that is less than the specified value of the classification threshold *T*:

$$e_i(k,m,l,T)=\begin{cases}1, \tau(i,i,k,m,l)<T\\ 0, \tau(i,i,k,m,l)\geq T\end{cases}. \quad (7)$$

The error in between-class distance measuring (type I error or a false positive measure) [17] is the value of the between-class distance which is greater than the specified value *T*:

$$e_{ij}(k,m,l,T)=\begin{cases}1, \tau(i,j,k,m,l)>T\\ 0, \tau(i,j,k,m,l)\leq T\end{cases}. \quad (8)$$

It is clear from formulas (7) and (8) that an increase in the threshold value *T* reduces in the number of type I errors but concurrently increases in the number of type II errors and vice versa.

The optimal value for each aircraft class corresponds to the minimum number of type I and II errors for the given range of the vector-contour elements quantity *l*.

The relative type II measurement error (the ratio of the within-class distance measurement errors to their total number) for the *i*-th class with the given *l* and *T* is defined as:

$$E_{IC}(i,l,T)=\frac{N_{IC}(i,l,T)}{N_i\cdot(N_i-1)}, \quad (9)$$

$$\mathrm{N}_{IC}(i,l,T)=\sum_{k=1}^{N_i}\sum_{m=1,m\neq k}^{N_i}e_i(k,m,l,T), \quad (10)$$

where $\mathrm{N}_{IC}(\cdot)$ – is the number of type II measurement errors.

The relative type I measurement error (the ratio of the between-class distance measurement errors to their total number) is calculated with the formula:

$$E_{BC}(i,l,T)=\frac{N_{BC}(i,l,T)}{N_i\cdot\sum_{j=1,j\neq i}^{N_C}N_j}, \quad (11)$$

$$N_{BC}(i,l,T)=\sum_{j=1,j\neq i}^{N_C}\sum_{k=1}^{N_i}\sum_{m=1}^{N_j}e_{ij}(k,m,l,T), \quad (12)$$

where $N_{BC}(\cdot)$ – is the number of type I measurement errors.

At each classification threshold value, the total relative measurement error $E_{\min}(\cdot)$ is calculated as a minimal sum of relative type I and II measurement errors and represents an objective function [18] to compute an optimal threshold value T for C_i class:

$$E_{\min}(i,T) = \min_{l}\left(E_{IC}(i,l,T) + E_{BC}(i,l,T)\right). \quad (13)$$

The vector-contour elements quantity l varies within the interval $l = [100,...1000]$ with a step of 10. The interval boundaries are explained by the fact that the distinguishing features of the most aircraft in the training dataset are lost at $l < 100$, and $l > 1000$ reaches the minimum quantity of items for some reference instances.

The classification threshold changes within the interval $T = [60,...,80]$ with a step of 1. The interval is chosen according to the following arguments: at $T < 60\%$ many instances of different classes are similar to each other, whereas at $T > 80\%$ a within-class similarity becomes insufficient due to the variety of contour shapes within a single class.

The experimental data was used to create graphs of the total relative measurement error (13) dependence from the classification threshold for each aircraft class. The graphs shown in Figure 5 provide the characteristic features of the most interesting classes of the training dataset. The B-1 class is described by significant differences between its instances, which is confirmed by high values of (13) in the range of 6-12% for the entire graph in Figure 5a with a slight predominance of type II measurement error. The B-52 class graph, on the contrary, demonstrates a rapid decline in type I error at a threshold of 60-70% with the following near-zero type II error on the right side of the graph.

As for the C-130 and P-3 classes of propeller aircraft (Figure 5b), the outwardly similar contours are characterized by close graphs of (13) with the predominance of type I error for C-130 and type II error for P-3.

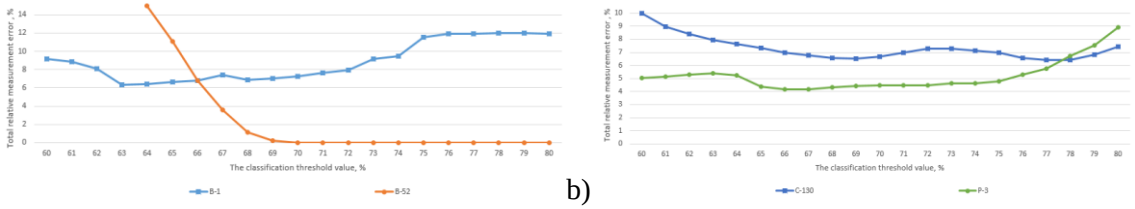

a) b)

Figure 5. Total relative measurement error (13) dependence from the classification threshold for classes B-1 / B-52 (a) and C-130 / P-3 (b).

Formula (13) was used to calculate the optimal classification thresholds $\mathbf{T} = \{T_i\}_{i=1}^{N_C}$ for each class in the training dataset (the results of the calculation are given in Table 3):

$$T_i = \arg\left[\min_{T}(E_{\min}(i,T))\right]. \quad (14)$$

Table 3. Optimal classification thresholds.

Class index	1	2	3	4	5	6	7	8
Class name	B-1	B-52	C-5	C-37	C-130	C-135	P-3	S-3
Optimal value T_i, %	63	71	66	69	69	69	66	74

5. Optimal vector-contour's items quantity calculation

The optimal values of vector-contour's items $\mathbf{L} = \{l_i\}_{i=1}^{N_C}$ for each aircraft class are calculated on the basis of the total relative measurement error using the previously determined threshold $\mathbf{T} = \{T_i\}_{i=1}^{N_C}$.

The sum of the relative measurement errors of type I (9) and II (11) errors represents an objective function to compute an optimal value of the items' quantity l_i for C_i class:

$$E(i,l) = E_{IC}(i,l,T_i) + E_{BC}(i,l,T_i). \quad (15)$$

Graphs (Figures 6-7) show the vector-contour's items optimal quantity corresponding to the minimum of (15) marked with a vertical line. The optimal items quantity for B-1 class (Figure 6a) lies near the intersection of the types I and II error graphs. The errors for a given class vary widely due to

the significant differences in its instances. The B-52 class items optimal quantity (Figure 6b) is determined only by the minimum of type I errors.

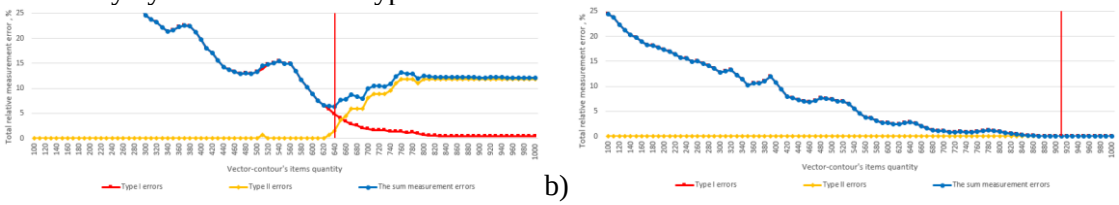

a) b)

Figure 6. Total relative measurement error (15) dependence from the B-1 (a) and B-52 (b) vector-contour's items quantity.

The optimal value of C-130 (Figure 7a) and P-3 (Figure 7b) classes biased towards type II error and is to the right of the intersection of both error graphs. Class C-130 is characterized by a higher total error value compared to P-3 due to more significant differences between the references instances of this class.

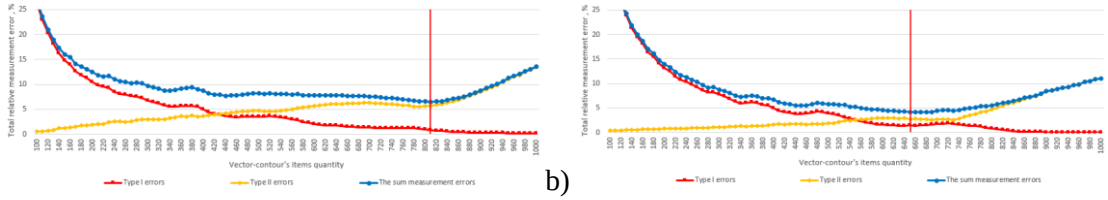

a) b)

Figure 7. Total relative measurement error (15) dependence from the C-130 (a) and P-3 (b) vector-contour's items quantity.

Formula (15) was used to determine the optimal values of vector-contour's items quantity $\mathbf{L} = \{l_i\}_{i=1}^{N_C}$ for each class in the training dataset (the results are presented in Table 4):

$$l_i = \arg\left[\min_{l}(E(i,l))\right]. \quad (16)$$

Table 4. Optimal values of the vector-contour's items quantity.

Class index	1	2	3	4	5	6	7	8
Class name	B-1	B-52	C-5	C-37	C-130	C-135	P-3	S-3
Optimal value l_i	640	910	900	910	810	680	650	580

The proposed optimal items' quantity calculation method was experimentally compared to the most widely used heuristic methods including the use of:

(a) the minimal items' quantity of the certain class's instances to minimize the type II error;
(b) the maximal items' quantity of the certain class's instances to minimize the type I error;
(c) the recognized object's items quantity to retain its actual level of details.

The table 5 represents the total relative measurement error (15) per each aircraft class along with the mean value for all the heuristic methods and the proposed one.

Table 5. The total relative error for the proposed method and for heuristics.

Row name	Total relative error (15), %								
Class index	1	2	3	4	5	6	7	8	Mean error through all classes
Class name	B-1	B-52	C-5	C-37	C-130	C-135	P-3	S-3	
Heuristic (a)	12.18	20.00	38.66	0.09	13.68	7.59	11.97	8.38	14.07
Heuristic (b)	12.18	13.33	26.29	0.09	21.23	3.70	10.00	3.97	11.35
Heuristic (c)	11.49	8.89	19.29	0.15	11.42	2.53	7.32	2.58	7.96
Proposed method	**9.42**	**0.00**	**2.13**	**0.00**	**6.51**	**0.23**	**4.18**	**0.76**	**2.90**

The differences in results of heuristic methods (a-c) for certain classes emphasize the training dataset's irregularity. The best heuristic solution is to use items' quantity of the recognized object, however, the proposed tuning method provides around 3 times less total measurement error.

6. Criterion for similarity value calculation

To estimate the developed parameters tuning method and to select a criterion for the similarity value calculation of a recognized vector-contour Γ to a set of reference instances $\mathbf{\Gamma}_i$, we used the test dataset described in section 2. The test images of 0.3/0.5 meters per pixel resolution are upscaled to 0.15 hence the instances of a certain class have close items' quantities through the whole dataset.

The recognition results for the test datasets obtained by the classification rule (4) in combination with the functions for similarity value calculation f_1 (5) and f_2 (6) are presented in Table 6.

Table 6. The results of test datasets recognition with the classification rule (4) in combination with functions f_1 and f_2.

Class index		1	2	3	4	5	6	7	8	Total
Class name		B-1	B-52	C-5	C-37	C-130	C-135	P-3	S-3	
f_1	Type I errors	0	0	3	0	3	0	1	0	7 (1.66%)
	Type II errors	1	0	0	0	0	0	0	0	1 (0.24%)
	Total errors	*1*	*0*	*3*	*0*	*3*	*0*	*1*	*0*	**8 (1.9%)**
f_2	Type I errors	1	0	2	0	0	29	0	0	32 (7.6%)
	Type II errors	5	5	6	11	45	39	31	1	143 (33.9%)
	Total errors	*6*	*5*	*8*	*11*	*45*	*68*	*31*	*1*	**175 (41.5%)**

Function (5) performs much better than (6) that is explained by the fact our parameters tuning method uses a similar to (5) pair-wise within-class and between-class distance calculation rule to define type I and II measurement errors.

To reduce errors number we modified the classification rule (4) to combine the functions (5) and (6), integrate their merits and mutually compensate shortcomings. The modified classification rule becomes the following:

$$C(\Gamma)=\begin{cases} C_i : i=\arg\left[\max_i(f_2(\Gamma,\mathbf{\Gamma}_i)\ge T_i)\right], \\ C_i : i=\arg\left[\max_i(f_1(\Gamma,\mathbf{\Gamma}_i)\ge T_i)\right],\ \forall i\ \max_i f_2(\Gamma,\mathbf{\Gamma}_i)<T_i\ , \\ \varnothing : \forall i\ \max_i f_1(\Gamma,\mathbf{\Gamma}_i)<T_i, \end{cases} \tag{17}$$

The results of the test datasets recognition with the modified classification rule (17) are presented in Table 7.

Table 7. Test dataset recognition results with modified classification rule (17).

Class index		1	2	3	4	5	6	7	8	Total
Class name		B-1	B-52	C-5	C-37	C-130	C-135	P-3	S-3	
$f_1 + f_2$	Type I errors	0	0	1	0	0	0	0	0	1 (0.24%)
	Type II errors	1	0	0	0	0	0	0	0	1 (0.24%)
	Total errors	*1*	*0*	*1*	*0*	*0*	*0*	*0*	*0*	**2 (0.48%)**

The remaining type II error for the contour analysis method belongs to class B-1 and indicates the need to expand its training dataset with instances of the operating (non-disassembled) aircraft. The type I error for C-5 is explained by the segmentation algorithm fault.

7. Conclusion and discussion

In this paper, we presented the results of the experiment aimed to tune the contour analysis method to recognize aircraft on aerial imagery. We calculated optimal values of the vector-contour's items quantity and the classification threshold through measuring within- and between-class distances for all possible training set instances combinations with the following detecting and minimization of type I and II errors. It is shown that each class has its own optimal values of these parameters due to the features of the reference instances of the training dataset. We proposed a classification rule that combines the merits of functions based on the best instance match and the mean CCF for class respectively.

The vectors of further research are the development of new segmentation methods that allow solving the aircraft edges detection problem upon the conditions of camouflage, poor contrast with the underlying surface, illuminated and shaded areas, as well as close-lying airfield equipment.

8. References

[1] Furman Ya A, Krevetskii A V and Peredreev A K 2002 *An Introduction to Contour Analysis: Applications to Image and Signal Processing* (Moscow: Fizmatlit) p 592
[2] Furman Ya A, Yuriev A N and Yanshin V V 1992 *Digital Methods for Processing and Recognizing Binary Images* (Krasnoyarsk: Publishing House of Krasnoyarsk University) p 248
[3] Hsieh J W, Chen J M, Chuang C H and Fan K C 2005 Aircraft type recognition in satellite images *Vision, Image and Signal Processing* **152** 307-315
[4] Liu G, Sun X, Fu K and Wang H 2013 Aircraft recognition in high-resolution satellite images using coarse-to-fine shape prior *IEEE Geoscience and Remote Sensing Letters* **10** 573-577
[5] Wu Q, Sun H, Sun X, Zhang D, Fu K and Wang H 2015 Aircraft recognition in high-resolution optical satellite remote sensing images *IEEE Geoscience and Remote Sensing Letters* **12** 112-116
[6] Veltkamp R C 2001 Shape matching: similarity measures and algorithms *Proc. Int. Conf. on Shape Modeling and Applications* (Geneva: SMI) 188-197
[7] Gostev I M 2010 Geometric correlation methods for the identification of graphical objects *Physics of Particles and Nuclei* **41** 27-53
[8] Zakharov A A, Barinov A E, Zhiznyakov A L and Titiv V S 2018 Object Detection in Images with a Structural Descriptor Based on Graphs *Computer Optics* **42(2)** 283-290 DOI: 10.18287/2412-6179-2018-42-2-283-290
[9] Ronneberger O, Fischer P and Brox T 2015 U-net: convolutional networks for biomedical image segmentation *Int. Conf. on Medical Image Computing and Computer-Assisted Intervention* **9351** 234-241
[10] He K, Zhang X, Ren S and Sun J 2016 Deep residual learning for image recognition *Conf. on Computer Vision and Pattern Recognition* (Las Vegas: Conference Publishing Services) 770-778
[11] Pan S J and Yang Q 2010 A survey on transfer learning *Transactions on Knowledge and Data Engineering* **22** 1345-1359
[12] Miroshnichenko S Yu, Degtyarev S V and Titov V S 2009 Detection of object edges in aerospatial cartographic images *Machine Graphics & Vision* **18** 427-437
[13] Gorbachev S V, Emelyanov S G, Zhdanov D S, Miroshnichenko S Y, Syryamkin V I, Titov D V and Shashev D V 2018 *Digital Processing of Aerospace Images* (London: Red Square Scientific, Ltd) p 244
[14] Gonzales R and Woods R 2002 *Digital Image Processing* (London: Pearson Education) p 793
[15] Blokhinov Y B, Gorbachev V A, Rakutin Y O and Nikitin A D 2018 A Real-Time Semantic Segmentation Algorithm for Aerial Imagery *Computer Optics* **42(1)** 141-148 DOI: 10.18287/2412-6179-2018-42-1-141-148
[16] Wikipedia Davis-Monthan Air Force Base URL: https://en.wikipedia.org/wiki/Davis–Monthan_Air_Force_Base (01.02.2019)
[17] Flach P 2012 *Machine Learning: the Art and Science of Algorithms that Make Sense of Data* (Cambridge University Press) p 396

[18] Singiresu S R 2009 *Engineering Optimization: Theory and Practice* (John Wiley & Sons) p 840

Acknowledgments
The authors gratefully acknowledge support by CodLix LLC.